Kanoje et al. 2017. *Int. J. Vehicle Structures & Systems*, 9(3), 154-163
ISSN: 0975-3060 (Print), 0975-3540 (Online)
doi: 10.4273/ijvss.9.3.05

International Journal of Vehicle Structures & Systems
Available online at www.maftree.org/eja

Creep Forces Effect on the Ride of Empty Indian Freight Wagon

Nagvendra Kumar Kanoje[a], Satish C. Sharma[b] and Suraj P. Harsha[c]

Mech. Industrial and Engg. Dept., Indian Institute of Tech., Roorkee, Uttarakhand, India
[a]Corresponding Author, Email: nagvendrakanoje@gmail.com
[b]Email: sshmefme@iitr.ernet.in
[c]Email: surajfme@iitr.ernet.in

ABSTRACT:

Indian Freight system is facing huge competition. The average speed of wagons at 40-50 kmph for empty wagons faces huge hunting problem. In these paper Indian parameters are studied using a numerical model The numerical model is consist of a whole wagon with two conventional three-piece bogie running on wheelsets. The wheel-rail contact is considered with heuristic nonlinear creep model for both single point and two point contact. Coulomb friction model is considered for contact between the truck and bolster. The present study concentrates on the critical hunting which is mainly depending on primary and secondary suspension parameters. A numerical study is run in Matlab to obtain the optimum parameters for increasing critical speed to stabilize wagon for both increased speed and at loaded vehicle.

KEYWORDS:

Hunting; Rail; Bogie; Freight wagon; Contact; Critical speed; Matlab

CITATION:

N.K. Kanoje, S.C. Sharma and S.P. Harsha. 2017. Creep Forces Effect on the Ride of Empty Indian Freight Wagon, *Int. J. Vehicle Structures & Systems*, 9(3), 154-163. doi:10.4273/ijvss.9.3.05.

1. Introduction

Hunting is common lateral instability caused during the running of vehicle. It basically arises from the interaction of inertial forces and adhesion forces. At low speed, adhesion dominates but, as the speed increases, the adhesion forces and inertial forces become comparable in magnitude and the oscillation begins at a "critical speed". The severe hunting motion will deteriorate the running quality of the train, reduce ride comfort and may cause derailment of the vehicle. The coning of wheel tread profile was first well understood by George Stephenson in 1821 [29] which lead to kinematic oscillation. The frequent and uncontrolled oscillation leads to instability which was firstly considered by De Pater [1]. Cooperrider [2] first formulated the dynamic system which considered the longitudinal, lateral but not the spin creep forces to describe the lateral dynamics of the bogie. Later Knudesen et al [3] investigated the chaotic behaviour of wheelset by considering the nonlinear friction laws of rolling contact. Knudesen et al [4] also continue study with the effect of speed and suspension and flange stiffness's on the dynamic of wheelset by calculation of Lyapunov exponent.

Kaas-Petersen et al [5] studied the hunting motions of the Cooperrider bogie with and without flange forces, true et al [6-8] studied the above models bifurcation behavior and analysed the nonlinear railway vehicle system. Ahmadian et al [9-10] investigated the hunting stability considering nonlinear yaw dampers and wheel-rail contact forces. Preben et al [11] did investigation of the Cooperrider's bogie for ultimate transition to chaos at a very high speed described it as Type-1. Carsten et al [12] find the generic bifurcations from a symmetric periodic solution of the model for various bifurcations. The interaction between wheel-rail mainly consists of contact forces due to creep and spin moments play important role in dynamic stability of railway vehicle. In case of wheel-rail contact many theories such as Kalker's linear theory, the Vermeulen and Johnson model and heuristic nonlinear models have been utilized to investigate the contact area and contact forces which are important parameters for controlling stability against hunting oscillations.

Wicken [13] first studied the dynamic instability caused due to interaction of the conicity of the wheels and the creep forces acting between the wheels and rails. Assuming small creepage and spin, Kalker [14] presented linear relations between creep forces and moments, and creepages. Stephan et al [15] have shown the loss of steering loss due to various wheel-rail contact conditions with the help of theoretical and experimental demonstration. Kovalev et al [16] presented a mathematical model for the nonlinear contact forces created in non-elliptical contact between railway vehicles and rails. Rajasekaran *et al* [17] studied structural performance using various material alternatives to arrive at the optimal performance and mass savings. Polach studied the dynamics of railway vehicle at adhesion limit of creep forces for wheel-rail interaction. Pombo et al [19] compared tangential creep forces and moments evaluated using Kalker's linear theory, a heuristic non-linear model and the formulation presented by Polach [20]. There was much numerical work in the past but the Robert F. Harder [21] developed a load-dependent friction wedge model using the

ADAMS/VIEW environment and simulation is run for bogie dynamics under different operating conditions.

Bosso et al [22] was the first to model a freight vehicle in Adams environment and tried to find the difference of riding when vehicle is empty or laden. The analytical model of whole vehicle can be created and can be simulated in MATLAB. Andrzej [23] give an idea that MATLAB can be a useful environment to build a user friendly interface for simulation of railway passenger. The dynamics of vehicle mainly depends on the wheel-rail interaction forces. The nature is complex due to the shape of the wheel and rail profiles. A contact zone has both adhesion and slip zone and due to this it is contrary to control the shape of contact zone. The creep forces occur in the contact zone are of highly nonlinear nature. Nowadays computational model of whole railway dynamics and wheel-rail interaction are getting wonderful measures for doing analysis. These models give proper understanding and determination of the various parameters for the control of creep forces and the stability of vehicle.

This paper proposes to find out the optimum critical speed for the Indian freight empty wagon. The Indian parameters [26] are fed in to the numerical model of Anant [24,25] considering the heuristic nonlinear creep model. The railway vehicle has 42-DOF freedom which considers lateral and yaw displacement, lateral and yaw velocity of the wheelset, truck and car body and lateral displacement of the left and right rail. It considers nonlinearity in wheel-rail profile and also nonlinear suspension of the wheelset. The critical velocity is determined and phase plots, orbit plots and displacement plots of the wheelset at different speeds are plotted to understand the stable behaviour of the wheelset.

2. Wheelset model and mathematical formulation

The wheelset represents the basic element of the rail vehicle steering and support system. Each wheelset consists of two steel wheels rigidly mounted to a solid axle. In this paper we make use of the AAR 1 in 20 wheel. The mathematical formulation for a single wheelset model which is taken from Anant Mohan [24-25] is used. The forces and moments which act on a single wheelset are governed by the lateral and yaw motions of the wheelset. The wheelset is suspended by springs and viscous dampers in a fixed frame that has no lateral or vertical displacements. The single wheelset is subjected to specific initial conditions. Both single-point and two-point wheel/rail contact conditions were considered. The simulation software MATLAB was used to find time-domain solutions to the wheelset dynamic equations. The numerical model here is considered is from Anant [25]. In this formulation consider some assumption:

a) The track has no irregularities and defects.
b) The wheel to be rolling on a smooth, level, and straight track.
c) The radius of curvature of the track therefore is infinite and the track super elevation angle is zero.
d) The centrifugal forces and the cant insufficiency are zero.

The present formulation incorporates the track flexibility model in which each rail is assumed to have lateral freedom only. In this model, rail rollover or overturning motion is neglected. The rail is assumed to have effective lateral mass, viscous damping, and linear stiffness, m_{RAIL}, C_{RAIL}, and K_{RAIL} respectively. The rail lateral displacement y_{RAIL} is related to the net lateral wheel force by the rail equation of motion presented later. The wheelset roll angle and its rate of change are given as,

$$\Phi_W = \frac{(R_L - R_R)}{2a} \qquad \dot{\Phi} = (\lambda_L + \lambda_R)\frac{\dot{y_w}}{2a}$$

The wheel is approximated here to have a constant conicity λ equal to 0.125 up to a tread thickness of 8mm (flange clearance), followed by a sharp flange. For any lateral travel of the wheel up to the flange clearance the rise or fall of the wheel center from the horizontal will be linear, and the wheel is said to be operating in the 'Tread Region'. The actual wheel has a sharp rise in radius at this point. In this thesis, however, the rise of the flange is assumed to extend from y = y_{FC} = 0.008 m (i.e. 8 mm) till y = y_{FC} = 0.009 m (i.e. 9 mm). The diameter change from tread to flange is assumed to take place over a lateral distance of 1.0 mm to avoid problems in digital simulation.

3. Rail model

A simple spring-mass-damper model of the rail is assumed.

$$-F_{RAIL} = m_{RAIL}\ddot{y}_{RAIL} + C_{RAIL}\dot{y}_{RAIL} + K_{RAIL}y_{RAIL}$$

Where, $-F_{RAIL}$ is the force acting on the rail. Since these values are so high, the term m_{RAIL}, $\ddot{y}_{RAIL}$ is neglected, therefore, the force on the rail is calculated as.

$$-F_{RAIL} = C_{RAIL}\dot{y}_{RAIL} + K_{RAIL}y_{RAIL}$$

3.1. Single-point creep forces and moments

When the contact between wheel and rail occurs there is an extremely complex physical phenomenon when the stiff wheels with elasticity move forward on the stiff rails with elasticity at a certain speed. The stiff wheels slide relative to the stiff rails and therefore there is some velocity difference in the contact area between the wheels and the rails. The slip includes elastic deformation and rigid slip. The relative velocity or relative angular velocity in wheel-rail contact point normalized by the forward speed. Assuming the forward velocity to be a constant and the vehicle to be travelling in a straight line, and taking into account the roll ($\dot{\phi}$), pitch ($\dot{\theta}$), and yaw ($\dot{\psi}$), the longitudinal creepage, the lateral creepage and the spin creepage of left and right wheel axles are

$$\xi_{XL} = \frac{1}{V}[V - R_L\dot{\theta}_W - a\dot{\psi}_W]$$

$$\xi_{YL} = \frac{1}{V}\left[\dot{y}_W + R_L(\dot{\Phi}_W - \dot{\theta}_W\psi_W) - \dot{y}_{RAIL,L}\right] / \cos(\delta_L + \Phi_W)$$

$$\xi_{SPL} = \frac{1}{V}\left[-\dot{\theta}_W \sin(\delta_L + \Phi_W) + (\dot{\psi}_W + \Phi_W\dot{\theta}_W)\cos(\delta_L + \Phi_W)\right]$$

$$\xi_{XR} = \frac{1}{V}\left[V - R_R\dot{\theta}_W + a\dot{\psi}_W\right]$$

$$\xi_{YR} = \frac{1}{V}\left[\dot{y}_W + R_R\left(\dot{\phi}_W - \dot{\theta}_W\psi_W\right) - \dot{y}_{RAIL,R}\right] / \cos(\delta_R - \phi_W)$$

$$\xi_{SPR} = \frac{1}{V}\left[\dot{\theta}_W \sin(\delta_R - \phi_W) + (\dot{\psi}_W + \phi_W\dot{\theta}_W)\cos(\delta_R - \phi_W)\right]$$

Where $\delta_L, \delta_R, R_L, R_R$ and ϕ_W are the wheel/rail geometry illustrating parameters.

The presence of creep forces in contact patch regulates the displacement by producing oscillatory motion against the displacement in the lateral plane. The motion of vehicle also depends on the springs K_{PX} and K_{PY} and the damper C_{PX} and C_{PY}. There are four creep coefficients, viz. f_{11}, f_{12}, f_{22}, and f_{33}, which decide the creep forces and moment. These are calculated for a nominal value of the normal load according to Kalker's linear theory [26-27] and then reduced by 50%. The actual values depend on the normal load FN and are to be reduced to the actual using the following relations:

$$f_{11} = f_{11}^*(F_N/F_N^*)^{2/3}$$
$$f_{12} = f_{12}^*(F_N/F_N^*)$$
$$f_{22} = f_{22}^*(F_N/F_N^*)^{4/3}$$
$$f_{33} = f_{33}^*(F_N/F_N^*)$$

Where coefficients f_{ij}^* are the values of the creep coefficients at the normal load F_N, f_{ij}^* are the creep coefficients for the nominal load F*N. The creep coefficients are functions of the wheel/rail geometry, material properties and the normal load. Different papers have used different values for the coefficients. Assume values for simulation are $f_{11T} = 9.43\times10^6$N and $f_{33T} = 10.23\times10^6$N, $f_{12T} = 1.2$ kNm, $f_{22T} = 1$ kNm^2. Where the subscripts T and F refer to the tread and the flange values respectively [25].

The creep forces and the creep moments are produced by the relative slip of wheels and rails in the contact area and depend on the creepage. The creep forces and creep moments between the wheels and rails in a linear region can be expressed according to Kalker's linear creep theory [16, 17] is

$$F'_{CPX} = -f_{33}\xi_X$$
$$F'_{CPY} = -f_{11}\xi_y - f_{12}\xi_{SP}$$
$$M'_{CPZ} = f_{12}\xi_y - f_{22}\xi_{SP}$$

Of these forces, the force in the y direction opposes the velocity of the motion and being similar to a frictional force, can be beneficial in damping out oscillations. But the force in the x direction produces a torque, which will set up yaw motion and thus produces oscillatory motion, causing the wheelset to hunt between the rails. The direction of this torque is such that when the wheelset is moving towards the left, the yaw tends to turn the wheelset so as to cause the wheelset to move towards the right rail and vice versa, hence causing a hunting motion. It is found that for forward speeds below the critical speed, the disturbance caused by any initial perturbation dies out, while for forward speeds over the critical speed, the oscillation grows into a limit cycle, where the flanges start hitting against the rails.

The higher the forward speed over the critical speed, the more the wheel climbs the flange. Hence, the closer the wheel gets to derailment. Beyond the critical speed, oscillatory motion is observed even without the flange. The amplitude of the limit cycle varies with the value of the speed. The critical velocity is seen to vary inversely with the wheel conicity λ. But there is a limiting condition to the value of these forces. The resultant creep force cannot exceed that available due to adhesion. If F_N is the normal force at the rail contact patch, then the resultant of the creep forces F'_{CPX} and F'_{CPY} cannot exceed that due to available adhesion at the wheel / rail contact patch, i.e.

$$\sqrt{{F'_{CPX}}^2 + {F'_{CPY}}^2} \leq \mu F_N$$

In simulation, this condition is achieved by using a modified Vermeulen-Johnson model [1, 4 and 7]. In this method, which includes the effect of spin creepage, a saturation coefficient, ε is calculated at each of the three contact patches using the following relation:

$$\varepsilon = (1/\beta) \times [\beta - \beta^2/3 + \beta^3/27] \quad \text{For } \beta < 3$$
$$\varepsilon = 1/\beta \quad \text{For } \beta \geq 3$$

Where β is the normalized unlimited creep force, and ε is the saturation constant.

$$\beta = \frac{1}{\mu F_N} \times \sqrt{{F'_{CPX}}^2 + {F'_{CPY}}^2}$$

This condition is achieved by using a heuristic non-linear creep formulation model. The creep forces and moments for saturated contact patch (CP), left and right contact patch are then given by,

$$F_{CPX} = \varepsilon \times F'_{CPX}$$
$$F_{CPY} = \varepsilon \times F'_{CPY}$$
$$F_{CPZ} = \varepsilon \times F'_{CPZ}$$
$$F_{CXL} = F_{CPXL}$$
$$F_{CYL} = F_{CPYL}\cos(\delta_L + \phi_W)$$
$$F_{CZL} = F_{CPYL}\sin(\delta_L + \phi_W)$$
$$M_{CXL} = 0$$
$$M_{CYL} = -M_{CPZL.}\sin(\delta_L + \phi_W)$$
$$M_{CZL} = M_{CPZL}\cos(\delta_L + \phi_W)$$
$$F_{CXR} = F_{CPXR}$$
$$F_{CYR} = F_{CPYR}\cos(\delta_R - \phi_W)$$
$$F_{CYR} = -F_{CPYR}\sin(\delta_R - \phi_W)$$
$$M_{CXR} = 0$$
$$M_{CYR} = M_{CPZR}\sin(\delta_R - \phi_W)$$
$$M_{CZR} = M_{CPZR}\cos(\delta_R - \phi_W)$$

3.2. Single-point normal forces and moments

The normal forces at the two rails are required to be calculated at each time step, since the exact value of the normal force will depend on the angle of contact as well as the roll angle, they are.

$$F_{NL} = V_L/\Delta$$
$$F_{NR} = V_R/\Delta$$
$$V_L = F_Z^*\{a\cos(\delta_R - \phi_W) - R_R\sin(\delta_R - \phi_W)\} + M_\phi^*\cos(\delta_R - \phi_W)$$

$$V_R = F_Z^*\{a\cos(\delta_L + \phi_W) - R_L\sin(\delta_L + \phi_W)\} - M_\phi^*\cos(\delta_L + \phi_W)$$

$$\Delta = 2a\cos(\delta_L + \phi_W)\cos(\delta_R - \phi_W) - R_R\cos(\delta_L + \phi_W)\sin(\delta_R - \phi_W) - R_L\sin(\delta_L + \phi_W)\cos(\delta_R - \phi_W)$$

In the above expressions, F_Z^* and $M_\phi^*$are equivalent vertical force and equivalent roll moment given by.

$$F_Z^* = -F_{CZL} - F_{CZR} - F_{SUSPZW} + m_W g$$

$$M_\phi^* = a(F_{CZR} - F_{CZL}) - R_L(F_{CYL} - \psi_W F_{CXL}) - R_R(F_{CYR} - \psi_W F_{CXL}) - \psi_W(M_{CYL} + M_{CYR}) - I_{WY}\dot{\theta}_W\dot{\psi}_W$$

The normal forces on the left and right wheels, F_{NL} and F_{NR} act perpendicular to the contact patch plane and can be resolved into lateral and vertical components in the track plane.

$$F_{NYL} = -F_{NL}\sin(\delta_L + \phi_W)$$

$$F_{NZL} = F_{NL}\cos(\delta_L + \phi_W)$$

$$F_{NYR} = F_{NR}\sin(\delta_R - \phi_W)$$

$$F_{NZR} = F_{NR}\cos(\delta_R - \phi_W)$$

3.3. Single-point wheelset dynamic equation

The dynamic equations of a single wheelset are obtained from Newton's laws applied to the wheelset, both for force and moments. Thus the sum of all forces acting on the wheelset in the lateral and vertical directions will equal the product of the mass and the lateral and vertical accelerations respectively.

$$F_{CYL} + F_{CYR} + F_{NYL} + F_{NYR} + F_{SUSPYW} - m_W g\phi_W = m_W\ddot{y}_W$$

$$I_{WZ}\ddot{\psi}_W = -I_{WY}\dot{\theta}_W\dot{\phi}_W - a(F_{CXL} - F_{CXR}) - \psi_W\{(a - R_L\tan(\delta_L + \phi_W))(F_{CYL} + F_{NYL}) - (a - R_R\tan(\delta_R - \phi_W))(F_{CYR} + F_{NYR})\} + M_{CZL} + M_{CZR} + M_{SUSPZW} - \phi_W(M_{CYL} + M_{CYR})$$

$$C_{RAIL}\dot{y}_{RAIL,L} + K_{RAIL}y_{RAIL,L} = -F_{NYL} - F_{CYL}$$

$$C_{RAIL}\dot{y}_{RAIL,R} + K_{RAIL}y_{RAIL,R} = -F_{NYR} - F_{CYR}$$

3.4. Two-points wheel/rail contact

For the AAR 1 in 20 wheel, which has an abrupt flange, when the lateral wheelset excursion becomes equal to the flange clearance, both the tread and the flange of the wheel make contact with the rail. Hence, a two-point contact condition involves three different contact patches (two at the flanging wheel and one at the other wheel). The equations pertaining to the left and the right wheels, when the two-point contact condition occurs at the left wheel/rail interface are listed below. These equations can be similarly written for a two-point contact condition at the right wheel. The condition for the left rail to have two-point contact is then.

$$y_W - y_{RAIL,L} = y_{FC}$$

When the flange is touching the left rail, the velocity and acceleration of the wheel and rail will be the same, i.e.

$$\dot{y}_W = \dot{y}_{RAIL,L}$$

$$\ddot{y}_W = \ddot{y}_{RAIL,L}$$

3.5. Two-points creep forces & moments

Assuming the forward velocity to be a constant and the vehicle to be travelling in a straight line, and taking into account the roll ($\dot{\phi}$), pitch ($\dot{\theta}$), and yaw ($\dot{\psi}$), the longitudinal creepage, the lateral creepage and the spin creepage of left contact (tread and flange) and right contact (tread) patches are given by:

$$\xi_{XLT} = \frac{1}{V}\left[V - R_{LT}\dot{\theta}_W - a\dot{\psi}_W\right]$$

$$\xi_{YLT} = \frac{1}{V}\left[\dot{y}_W + R_{LT}\left(\dot{\phi}_W - \dot{\theta}_W\psi_W\right) - \dot{y}_{RAIL,L}\right] / \cos(\delta_{LT} + \phi_W)$$

$$\xi_{SPLT} = \frac{1}{V}\left[-\dot{\theta}_W\sin(\delta_{LT} + \phi_W) + (\dot{\psi}_W + \phi_W\dot{\theta}_W)\cos(\delta_{LT} + \phi_W)\right]$$

$$\xi_{XLF} = \frac{1}{V}\left[V - R_{LF}\dot{\theta}_W - a\dot{\psi}_W\right]$$

$$\xi_{YLF} = \frac{1}{V}\left[\dot{y}_W + R_{LF}\left(\dot{\phi}_W - \dot{\theta}_W\psi_W\right) - \dot{y}_{RAIL,L}\right] / \cos(\delta_{LF} + \phi_W)$$

$$\xi_{SPLF} = \frac{1}{V}\left[-\dot{\theta}_W\sin(\delta_{LF} + \phi_W) + (\dot{\psi}_W + \phi_W\dot{\theta}_W)\cos(\delta_{LF} + \phi_W)\right]$$

$$\xi_{XR} = \frac{1}{V}\left[V - R_R\dot{\theta}_W - a\dot{\psi}_W\right]$$

$$\xi_{YR} = \frac{1}{V}\left[\dot{y}_W + R_R\left(\dot{\phi}_W - \dot{\theta}_W\psi_W\right) - \dot{y}_{RAIL,R}\right] / \cos(\delta_R - \phi_W)$$

$$\xi_{SPF} = \frac{1}{V}\left[-\dot{\theta}_W\sin(\delta_R + \phi_W) + (\dot{\psi}_W + \phi_W\dot{\theta}_W)\cos(\delta_R - \phi_W)\right]$$

The angles of contact δ_T and δ_F as well as the rolling radii R_T and R_F for the tread and flange points of contact will be different.

3.6. The proposed non-linear creep model

Following Hertz contact theory, the shape of the contact area between rails and wheels are assumed to be elliptical. The values of all the parameters in new non-linear creep model are calculated in the same way as in single-point contact.

$$F_{CPX} = \varepsilon \times F'_{CPX}$$

$$F_{CPY} = \varepsilon \times F'_{CPY}$$

$$F_{CPZ} = \varepsilon \times F'_{CPZ}$$

The forces are calculated for the left tread, left flange and the right contact patches separately are.

$$F_{CXLT} = F_{CPXLT}$$

$$F_{CYLT} = F_{CPYLT}\cos(\delta_L + \phi_W)$$

$$F_{CZLT} = F_{CPYLT}\sin(\delta_L + \phi_W)$$

$$M_{CXLT} = 0$$

$$M_{CYLT} = -M_{CPZLT.}\sin(\delta_L + \phi_W)$$

$$M_{CZLT} = M_{CPZLT}\cos(\delta_L + \phi_W)$$

$$F_{CXLF} = F_{CPXLF}$$

$$F_{CYLF} = F_{CPYLF}\cos(\delta_L + \phi_W)$$

$$F_{CZLF} = F_{CPYLF}\sin(\delta_L + \phi_W)$$

$$M_{CXLF} = 0$$

$$M_{CYLF} = -M_{CPZLF.}\sin(\delta_L + \phi_W)$$

$$M_{CZLF} = M_{CPZLF}\cos(\delta_L + \phi_W)$$
$$F_{CXR} = F_{CPXR}$$
$$F_{CYR} = F_{CPYR}\cos(\delta_L + \phi_W)$$
$$F_{CZR} = F_{CPYR}\sin(\delta_L + \phi_W)$$
$$M_{CXR} = 0$$
$$M_{CYR} = -M_{CPZR.}\sin(\delta_L + \phi_W)$$
$$M_{CZR} = M_{CPZR}\cos(\delta_L + \phi_W)$$

The forces acting on the wheel depend on the point or points where the wheel comes in contact with the rail. The flange clearance is assumed to be 8mm (0.32in). When the wheelset excursion is less than the flange clearance, tread contact occurs. When the wheelset excursion equals or exceeds the flange clearance, flanging occurs. There is a small region, where two-point contact occurs, both the tread and the flange are in contact with the rail. While the flange rises very sharply in the actual wheel, the profile used in the simulation assumes a lateral wheel travel of 1mm (between 8mm and 9mm total wheelset excursion during which two-point contact occurs.

3.7. Two–points contact normal forces & moments

Assuming two-point contact condition at the left wheel/rail interface, the normal forces at the left tread, left flange and right tread are.

$$F_{NLT} = V_{LT}/\Delta 2$$
$$F_{NLF} = V_{LF}/\Delta 2$$
$$F_{NR} = V_{2R}/\Delta 2$$
$$V_{LT} = F'_Y\{2a\cos(\delta_{LF} + \phi_W)\cos(\delta_R - \phi_W) - R_{LF}\sin(\delta_R - \phi_W)\cos(\delta_R - \phi_W) - R_R\cos(\delta_{LF} + \phi_W)\sin(\delta_R - \phi_W)\} + F''_Z\{\sin(\delta_{LF} + \phi_W)[a\cos(\delta_R - \phi_W) - R_R\sin(\delta_R - \phi_W)]\} + M''_\phi\cos(\delta_R - \phi_W)\sin(\delta_{LF} + \phi_W)$$
$$V_{LF} = F''_Y\{-2a\cos(\delta_{LT} + \phi_W)\cos(\delta_R - \phi_W) - R_{LT}\sin(\delta_{LT} + \phi_W)\cos(\delta_R - \phi_W) + R_R\cos(\delta_{LT} + \phi_W)\sin(\delta_R - \phi_W)\} - F''_Z\{\sin(\delta_{LT} + \phi_W)[a\cos(\delta_R - \phi_W) - R_R\sin(\delta_R - \phi_W)]\} - M''_\phi\sin(\delta_{LT} + \phi_W)\cos(\delta_R - \phi_W)$$
$$V_{2R} = F''_Y\{R_{LF}\cos(\delta_{LT} + \phi_W)\sin(\delta_{LF} + \phi_W) - R_{LT}\sin(\delta_{LT} + \phi_W)\cos(\delta_{LF} + \phi_W)\} - M''_\phi\{\cos(\delta_{LT} + \phi_W)\sin(\delta_{LF} + \phi_W) - \sin(\delta_{LT} + \phi_W)\cos(\delta_{LF} + \phi_W)\} + F''_Z\{a[\cos(\delta_{LT} + \phi_W)\sin(\delta_{LF} + \phi_W) - \sin(\delta_{LT} + \phi_W)\cos(\delta_{LF} + \phi_W)]\} + (R_{LT} - R_{LT})\sin(\delta_{LT} + \phi_W)\sin(\delta_{LF} + \phi_W)$$
$$\Delta 2 = [2a\cos(\delta_R - \phi_W) - R_R\sin(\delta_R - \phi_W)]\{\cos(\delta_{LT} + \phi_W)\sin(\delta_{LF} + \phi_W) - \sin(\delta_{LT} + \phi_W)\cos(\delta_{LF} + \phi_W)\} + (R_{LF} + R_{LT})\sin(\delta_{LT} + \phi_W)\sin(\delta_{LF} + \phi_W)\cos(\delta_R - \phi_W)$$

F''_Y and F''_Z are the equivalent lateral forces and M''_ϕ is an equivalent roll moment given by the following expressions.

$$F^{**}_Y = -F_{CYLT} - F_{CLLF} - C_{RAIL}\dot{y}_W - K_{RAIL}(y_W - y_{FC})$$
$$F^{**}_Z = -F_{CZLT} - F_{CZLF} - F_{CZR} - F_{SUSPZW} + m_W g$$
$$M^{*}_\phi = a(F_{CZLT} + F_{CZLF} - F_{CZR}) - R_{LT}(F_{CYLT} - \psi_W F_{CXLT}) - R_{LF}(F_{CYR} - \psi_W F_{CXR}) - R_R(F_{CYR} - \psi_W F_{CXL}) - \psi_W(M_{CYLT} + M_{CYLF} + M_{CYR}) - I_{WY}\dot{\theta}_W\dot{\psi}_W$$

The resolved normal force components are as follows,

$$F_{NYLT} = -F_{NLT}\sin(\delta_{LT} + \phi_W)$$
$$F_{NZLT} = F_{NLT}\cos(\delta_{LT} + \phi_W)$$
$$F_{NYLF} = -F_{NLF}\sin(\delta_{LF} - \phi_W)$$
$$F_{NZLF} = F_{NLF}\cos(\delta_{LF} - \phi_W)$$
$$F_{NYR} = F_{NR}\sin(\delta_R - \phi_W)$$
$$F_{NZR} = F_{NR}\cos(\delta_R - \phi_W)$$

3.8. Two-points wheelset dynamic equations

The dynamic equations of a single wheelset are obtained from Newton's laws applied to the wheelset, both for force and moments. Thus the sum of all forces acting on the wheelset in the lateral and vertical directions will be equal to the product of the mass and the lateral and vertical accelerations respectively. Similarly, the sum of moments acting about any axis will equal the product of the mass moment of inertia and the angular acceleration.

$$F_{CYLT} + F_{CYLF} + F_{CYR} + F_{NYLT} + F_{NYLF} + F_{NYR} + F_{SUSPYW} - m_W g\phi_W = m_W\ddot{y}_W$$

$$I_{WZ}\ddot{\psi}_W = -I_{WY}\dot{\theta}_W\dot{\psi}_W - a(F_{CXLT} + F_{CXLF} - F_{CXR}) - \psi_W\{(a - R_{LT}\tan(\delta_{LT} + \phi_W))(F_{CYLT} + F_{NYLT}) + (a - R_{LF}\tan(\delta_{LF} + \phi_W))(F_{CYLF} + F_{NYLF}) - (a - R_R\tan(\delta_R + \phi_W))(F_{CYR} + F_{NYR})\} + M_{CZLT} + M_{CZLF} + M_{CZR} + M_{SUSPZW} + \phi_W(M_{CYLT} + M_{CYLF} + M_{CYR})$$

$$C_{RAIL}\dot{y}_{RAIL,L} + K_{RAIL}y_{RAIL,L} = -F_{NYLT} - F_{NYLF} - F_{CYLT} - F_{CYLF}$$
$$C_{RAIL}\dot{y}_{RAIL,R} + K_{RAIL}y_{RAIL,R} = -F_{NYR} - F_{CYR}$$

4. Wheelset suspension forces & moments

Suspension forces and moments act on each wheelset due to primary longitudinal and lateral suspension elements. Since this analysis neglects the wheelset vertical and roll degrees of freedom, the vertical suspension force and the roll suspension moment are assumed to be zero. The lateral suspension force and the yaw suspension moment acting on the leading wheelset of the truck are given by the expressions below.

$$F_{SUSPYW1} = -2K_{PY}y_{w1} + 2K_{PY}y_F + 2bK_{PY}\psi_F - 2C_{PY}\dot{y}_{w1} + 2C_{PY}\dot{y}_F - 2bC_{PY}\dot{\psi}_F$$
$$M_{SUSPYW1} = -2d_p^2K_{PX}\psi_{w1} + 2d_p^2K_{PX}\psi_F - 2d_p^2C_{PX}\dot{\psi}_{w1} + 2d_p^2C_{PX}\dot{\psi}_F$$

The lateral suspension force and the yaw suspension moment acting on the trailing wheelset (i = 2) of the truck are given by

$$F_{SUSPYW2} = -2K_{PY}y_{w2} + 2K_{PY}y_F + 2bK_{PY}\psi_F - 2C_{PY}\dot{y}_{w2} + 2C_{PY}\dot{y}_F - 2bC_{PY}\dot{\psi}_F$$
$$M_{SUSPYW2} = -2d_p^2K_{PX}\psi_{w2} + 2d_p^2K_{PX}\psi_F - 2d_p^2C_{PX}\dot{\psi}_{w2} + 2d_p^2C_{PX}\dot{\psi}_F$$

Suspension forces and moments act on the truck frame and the bolster due to the primary longitudinal and lateral suspension elements, as also the torsion Coulomb

damper between the truck frame and the bolster. The damper only allows yaw motion between the truck frame and the bolster. Figs. 3-4 show the secondary yaw suspension model. The lateral suspension force and the yaw suspension moment acting on the truck are given by the expressions below.

$$F_{SUSPYF1} = 2K_{PY}y_{w1} + 2K_{PY}y_{w2} - 4K_{PY}y_{F1} - 2K_{SY}y_{F1} + 2K_{SY}y_C + 2K_{SY}l_S\psi_C + 2C_{PY}\dot{y}_{w1} - 2C_{PY}\dot{y}_{w2} - 4C_{PY}\dot{y}_{F1} - 2C_{SY}\dot{y}_C + 2C_{SY}l_S\psi_C \quad (1)$$

$$M_{SUSPZF1} = 2bK_{PY}y_{w1} + 2d_p^2K_{PX}\psi_{w1} - 2bK_{PY}y_{w2} + 2d_p^2K_{PX}\psi_{w2} + (-4d_p^2K_{PX} - 4b^2K_{PY})\psi_{F1} + 2bC_{PY}\dot{y}_{w1} + 2d_p^2C_{PX}\dot{\psi}_{w1} - 2bC_{PY}\dot{y}_{w2} + 2d_p^2C_{PX}\dot{\psi}_{w2} + (-4d_p^2C_{PX} - 4b^2C_{PY})\dot{\psi}_{F1} - T_{COUL} \quad (2)$$

The lateral suspension force and the yaw suspension moment acting on the rear truck are given by the expressions below.

$$F_{SUSPYF2} = 2K_{PY}y_{w3} + 2K_{PY}y_{w4} - 4K_{PY}y_{F2} - 2K_{SY}y_{F2} + 2K_{SY}y_C - 2K_{SY}l_S\psi_C + 2C_{PY}\dot{y}_{w3} + 2C_{PY}\dot{y}_{w4} - 4C_{PY}\dot{y}_{F2} - 2C_{SY}\dot{y}_{F2} + 2C_{SY}\dot{y}_C - 2C_{SY}l_S\dot{\psi}_C \quad (3)$$

$$M_{SUSPZF2} = 2bK_{PY}y_{w3} + 2d_p^2K_{PX}\psi_{w3} - 2bK_{PY}y_{w4} + 2d_p^2K_{PX}\psi_{w4} + (-4d_p^2K_{PX} - 4b^2K_{PY})\psi_{F2} + 2bC_{PY}\dot{y}_{w3} + 2d_p^2C_{PX}\dot{\psi}_{w3} - 2bC_{PY}\dot{y}_{w4} + 2d_p^2C_{PX}\dot{\psi}_{w4} + (-4d_p^2C_{PX} - 4b^2C_{PY})\dot{\psi}_{F2} - T_{COUL} \quad (4)$$

The yaw suspension moment acting on the bolster is given by:

$$M_{SUSPZB1} = -K_{S\psi}\psi_{B1} + K_{S\psi}\psi_C - C_{S\psi}\dot{\psi}_{B1} - C_{S\psi}\dot{\psi}_C + T_{COUL} \quad (5)$$

The yaw suspension moment acting on rear bolster is given by:

$$M_{SUSPZB2} = -K_{S\psi}\psi_{B2} + K_{S\psi}\psi_C - C_{S\psi}\dot{\psi}_{B2} - C_{S\psi}\dot{\psi}_C + T_{COUL} \quad (6)$$

In Eqns. (4)-(6), T_{COUL} represents the Coulomb friction yaw moment acting on the truck frame due to interaction with the bolster. For numerical purposes, the model of the Coulomb friction is modified to include a linear viscous band at the origin. At low relative yaw rates between the bolster and the truck frame, the model assumes viscous damping. At higher relative yaw rates, the model assumes Coulomb damping with the frictional torque saturating at the centerplate breakaway value. This method approximates the frictional torque levels below T_O.

$$T_{COUL} = \begin{cases} T_o \dots\dots\dots\dots\dots\dots\dots\dots\dots\dots for\ (\dot{\psi}_F - \dot{\psi}_B) \geq T_o/C_o \\ C_o(\dot{\psi}_F - \dot{\psi}_B) \dots for\ -T_o/C_o < (\dot{\psi}_F - \dot{\psi}_B) < T_o/C_o \\ -T_o \dots\dots\dots\dots\dots\dots\dots\dots\dots\dots for\ (\dot{\psi}_F - \dot{\psi}_B) \leq -T_o/C_o \end{cases}$$

5. Carbody dynamics

Suspension forces act on the carbody due to its coupling with the front and the rear trucks. The trucks transmit motion to the carbody through secondary lateral, vertical, and yaw springs and dampers. Figs. 4-6 show the suspension forces and moments acting on the carbody. The suspension forces act on the carbody in the lateral direction. The suspension moments act in the yaw as well as the roll directions. These forces and moments are given by the following equations. Suspension force in the lateral direction due to the front truck and the rear truck:

$$F_{SUSPYC1} = 2K_{SY}y_{F1} - 2K_{PY}y_C + 2C_{SY}\dot{y}_{F1} - 2C_{SY}\dot{y}_C - 2h_{CS}K_{SY}\Phi_C - 2h_{CS}C_{SY}\dot{\Phi}_C$$

$$F_{SUSPYC2} = 2K_{SY}y_{F2} - 2K_{PY}y_C + 2C_{SY}\dot{y}_{F2} - 2C_{SY}\dot{y}_C - 2h_{CS}K_{SY}\Phi_C - 2h_{CS}C_{SY}\dot{\Phi}_C$$

Suspension moment in the yaw direction due to the front and the rear truck:

$$M_{SUSPZC1} = 2l_SK_{SY}y_{F1} + K_{S\psi}\psi_{B1} + (-2l_S^2K_{SY} - K_{S\psi})\psi_C + 2l_SC_{SY}\dot{y}_{F1} - C_{S\psi}\dot{\psi}_{B1} + (2l_S^2C_{SY} - C_{S\psi})\dot{\psi}_C$$

$$M_{SUSPZC2} = 2l_SK_{SY}y_{F2} + K_{S\psi}\psi_{B2} + (-2l_S^2K_{SY} - K_{S\psi})\psi_C + 2l_SC_{SY}\dot{y}_{F2} - C_{S\psi}\dot{\psi}_{B2} + (2l_S^2C_{SY} - C_{S\psi})\dot{\psi}_C$$

Suspension moment in the roll direction due to the front and the rear truck:

$$M_{SUSPXC1} = F_{SUSPYC1}h_{CS} - 2K_{SZ}d_s^2\phi_C - 2C_{SZ}d_s^2\dot{\phi}_C$$

$$M_{SUSPXC2} = F_{SUSPYC2}h_{CS} - 2K_{SZ}d_s^2\phi_C - 2C_{SZ}d_s^2\dot{\phi}_C$$

The lateral equation is obtained by applying the principle of linear momentum in the lateral direction [24]. Taking into account the lateral component of carbody weight and assuming small angles, the lateral equation of motion is given as:

$$\ddot{y}_c = (-m_cg\phi_c + F_{SUSPYC1} + F_{SUSPYC2})/m_c$$

The carbody yaw equation is obtained by applying the principle of angular momentum in the yaw direction. Assuming small angles, the carbody yaw equation of motion is given as:

$$\ddot{\psi}_C = (M_{SUSPZC1} + M_{SUSPZC2})/I_{CZ}$$

The carbody roll equation is obtained by applying the principle of angular momentum in the roll direction. Assuming small angles, the carbody roll equation of motion is given as:

$$\ddot{\phi}_C = (M_{SUSPXC1} + M_{SUSPXC2})/I_{CX}$$

6. Results and discussion

The simulation of mathematical formulation for whole single wagon with carbody, bogie and wheelset gives enough knowledge about the stability of the vehicle. The simulation is run for Indian freight empty wagon parameters as given in Table 1 and their influence is seen on stability of wagon by finding lateral displacement at various velocities. The forces and moments that act on the front and rear bogie and bolster and the wagon and which govern the lateral and yaw motion of the front and rear bogie and bolster and wagon were obtained and whole dynamics is understood. The result of numerical simulation is compared with VI-rail results. The influence of the primary and secondary stiffness for longitudinal and lateral degrees of freedom is diagnosed. For lower value of Kpx an empty wagon can have high critical velocity but the same wagon when loaded can't withstand low stiffness, Figs. 1(a)-(c), i.e. the wagon stiffness should be good for when it is empty and loaded.

The optimum value from simulation at 35m/s are Kpx = 3.6×10^6 and Kpy = 3.6×10^7.

Table 1: System parameters

Parameters	Value	Parameters	Value
Primary longitudinal stiffness	K_{PX} = various N/m	Centerplate breakaway torque	T_0 = 10168 N-m
Lateral suspension force on wheelset	F_{SUSPYW}	Half of track gauge	A = 0.717 m
Lateral suspension force on truck frame	F_{SUSPYF}	Acceleration due to gravity	g = 9.8 m/s^2
Primary lateral stiffness	K_{PY} = Various N/m	Lateral creep force coeff.	f_{11} = 9430000
Effective rail damping	C_{RAIL} = 14.6×10^4 N/m	Lateral/spin creep force coeff.	f_{12} = 1.2×10^3
Effective rail stiffness	K_{RAIL} = 14.67×10^7 N/m	Spin creep force coeff.	f_{22} = 1×10^3
Secondary lateral stiffness	K_{SY} = 2.345×10^6 N/m	Longitudinal creep force coeff.	f_{33} = 10.23×10^6
Secondary lateral damping	C_{SY} = 1.75×10^4 Ns/m	Mass of wheelset	m_W = 1595 kg
Secondary torsion stiffness	$K_{S\Psi}$ = 2.3275×10^6 N/m	Mass of bolster	m_B = 905 kg
Secondary torsion damping	$C_{S\Psi}$ =5×10^7Ns/m	Mass of truck frame	m_F = 603 kg
Secondary vertical stiff. Coeff.	K_{SZ} = 4.655×10^6 N/m	Mass of carbody	m_C = 9136 kg
Secondary vertical damp. coeff.	C_{SZ} = 1.75e4 Ns/m	Centered wheel rolling radius	r_O = 0.5m
Roll mass mom. of inertia of wheelset	I_{WX} = 1095 kgm^2	Primary longitudinal damping	C_{PX} = 36000 Ns/m
Pitch mass mom. of inertia of wheelset	I_{WY} = 131 kgm^2	Primary lateral damping	C_{PY} = 3600 Ns/m
Yaw mass mom. of inertia of wheelset	I_{WZ} = 1095 kgm^2	Wheel-rail flange clearance	y_{FC} = 0.0080 m
Yaw mass mom. of inertia of bolster	I_{BZ} =548 kgm^2	Coulomb friction yaw moment	T_{COUL}
Yaw mass mom. of inertia of truck frame	I_{FZ} =287 kgm^2	Lateral disp. of wheelset	y_W
Roll principal mass mom. of inertia of carbody	I_{CX} = 17799 kgm^2	Lateral disp. of truck frame	y_F
Yaw principal mass mom. of inertia of carbody	I_{CZ} = 101830 kgm^2	Lateral displacement of rail	y_{RAIL}
Longitudinal creep force on left wheel	F_{CXL}	Contact angle of left wheel	δ_L
Longitudinal creep force on right wheel	F_{CXR}	Contact angle of right wheel	δ_R
Half of Lateral distance between secondary vertical springs	d_S =0.5m	Coulomb viscous yaw damping coeff.	C_0 = 3.5×10^4 Ns/rad
Vertical distance between C.G. of carbody to secondary lateral springs	h_{CS} = 1.5m	Lateral tolerance added to yfc in order to facilitate simulation	y_{FCTOL} = 0.0010 m
Longitudinal distance between C.G. of carbody to C.G. of either truck	l_S = 5.25m	Half of distance between primary longitudinal springs	d_P = 0.61 m
Lateral creep force on left wheel	F_{CYL}	Rolling radius of left wheel	r_L
Lateral creep force on right wheel	F_{CYR}	Rolling radius of right wheel	r_R
Lateral normal force on left wheel	F_{NYL}	Wheelset roll angle	ϕ_W
Lateral normal force on right wheel	F_{NYR}	Yaw displacement of wheelset	ψ_W
Lateral creep moment on left wheel	M_{CYL}	Wheelset spin speed	$\dot{\theta}_W$
Lateral creep moment on right wheel	M_{CYR}	Wheel conicity	Λ = 0.125
Vertical creep moment on left wheel	M_{CZL}	Wheel-rail friction coeff.	m = 0.15
Vertical creep moment on right wheel	M_{CZR}	Young's modulus of material	E = 2.5e8
Vertical suspension moment on wheelset	M_{SUSPZW}	Poisson's ratio of material	υ = 0.3
Vertical suspension moment on bolster	M_{SUSPZB}	Axle load	N = 74530.5 N
Vertical suspension moment on truck frame	M_{SUSPZF}	Fwd. velocity of wheelset (m/s)	V = various

Table 2: Non-linear system parameters

Parameters	Value	Parameters	Value
Lateral creep force coeff.	f_{11}	Lateral suspension force on wheelset	F_{SUSPYW}
Lateral/spin creep force coeff.	f_{12}	Vertical suspension moment on wheelset	M_{SUSPZW}
Spin creep force coeff.	f_{22}	Rolling radius of left wheel	r_L
Longitudinal creep force coeff.	f_{33}	Rolling radius of right wheel	r_R
Creepage and spin coeff.	$C_{11}, C_{12}, C_{22}, C_{33}$	Contact angle of left wheel	δ_L
Semi-axis lengths of contact area	$\bar{a}, \bar{b}$	Contact angle of right wheel	δ_R

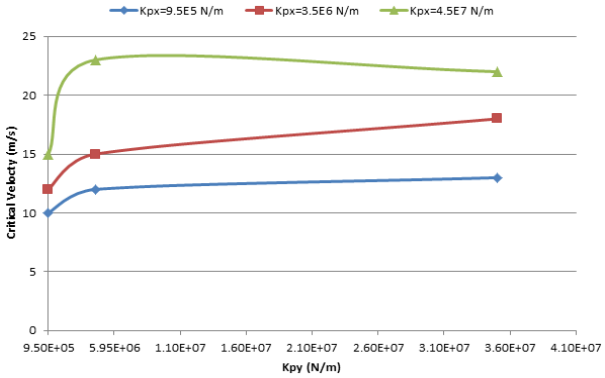

Fig. 1(a): Critical velocity vs. Kpy for Cpx = 30 kN/m^2

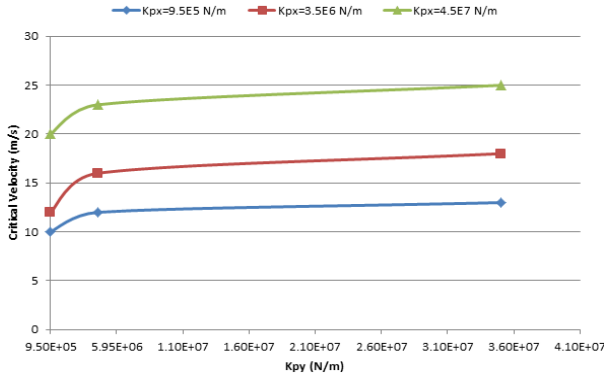

Fig. 1(b): Critical velocity vs. Kpy for Cpx = 36 kN/m^2

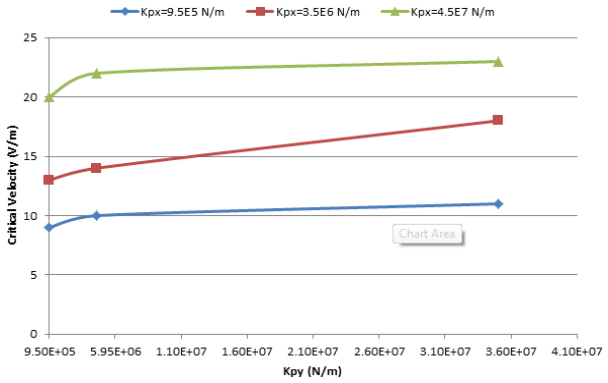

Fig. 1(c): Critical velocity vs. Kpy for Cpx = 100 kN/m^2 (bottom)

Fig. 2 shows the variation of Cpx for an increase in critical velocity. The value of Cpx can be easily controlled and the vehicle can easily become to stable nature because the nature of curve is linear. In Fig. 3, lower value of Cpy is quite stable. When we increase the value of Cpy to significant range, there is an increase in the critical velocity. There must be a mechanism to control the secondary lateral damping which is showing more significant improvement in the critical velocity. The increase in Cpy results in the increase of the critical velocity as shown in Fig. 4. It also shows that the Kpy value has an important significance. It shows that the value of Kpx and Kpy more than 1×10^7 decreases the critical speed. We can increase the critical velocity with proper control of primary and secondary stiffness for stable load. Fig. 5 shows that the variation of lateral secondary stiffness increases such that the excessive increase in Ksy decreases the critical velocity. It also shows more nonlinear behavior because of the curvilinear effects. Fig. 6 shows the variation of critical velocity against axle load. The behaviour is consistent with the other parameters studied so far.

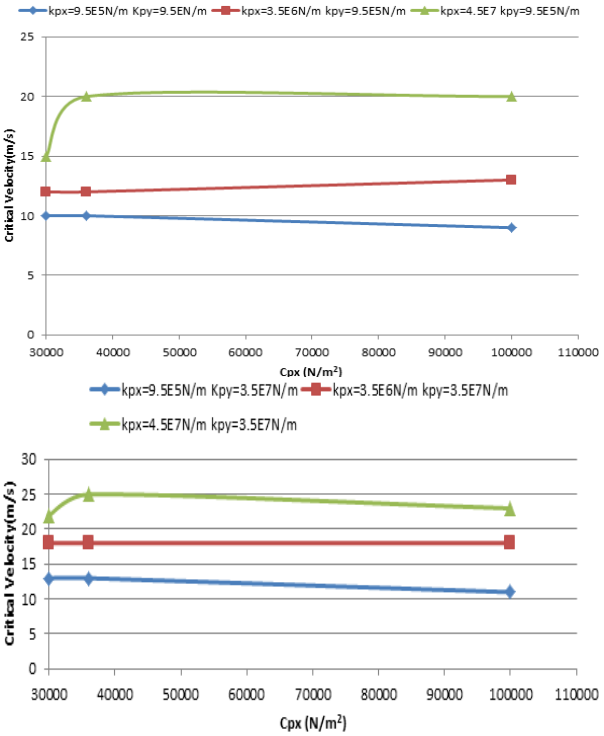

Fig. 2: Critical velocity vs. Cpx for range of Kpx and Kpy

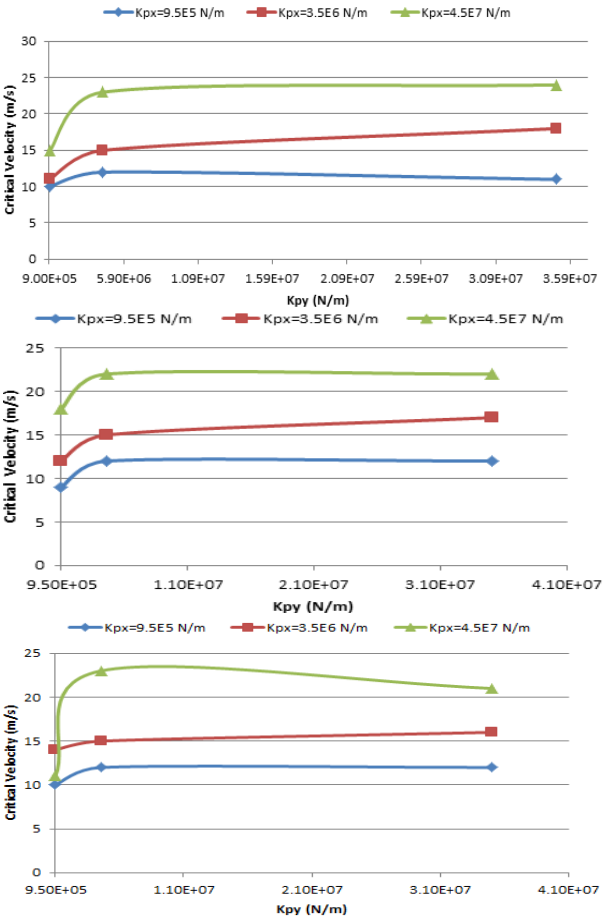

Fig. 3: Critical velocity vs. Kpy for Cpy = 3.6 kN/m^2 (top), Cpy = 15 kN/m^2 (middle) and Cpy = 36 kN/m^2 (bottom)

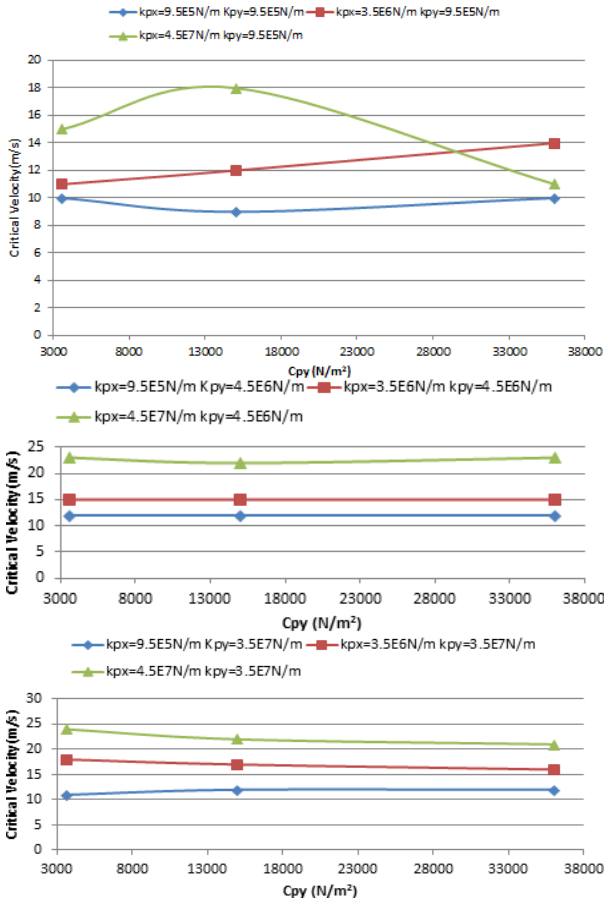

Fig. 4: Critical velocity vs. Cpy for range of Kpx and Kpy

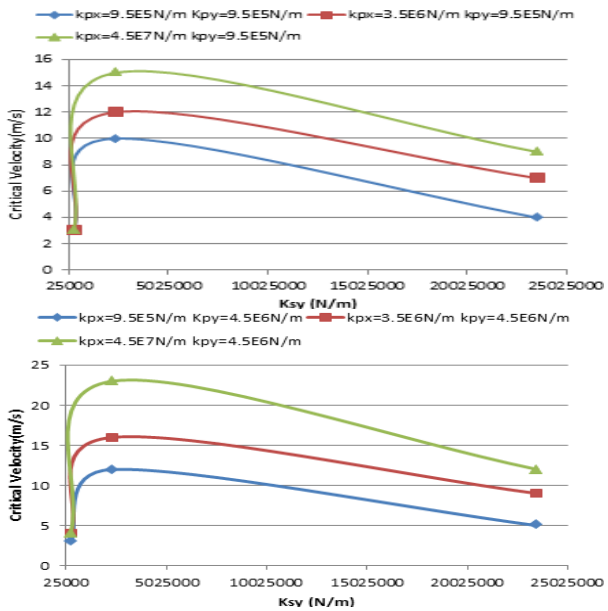

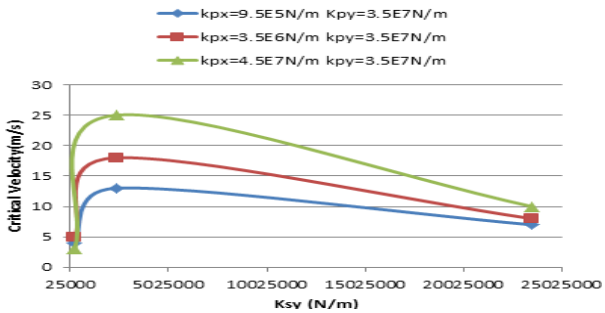

Fig. 5: Critical velocity vs. Ksy for range of Kpx and Kpy

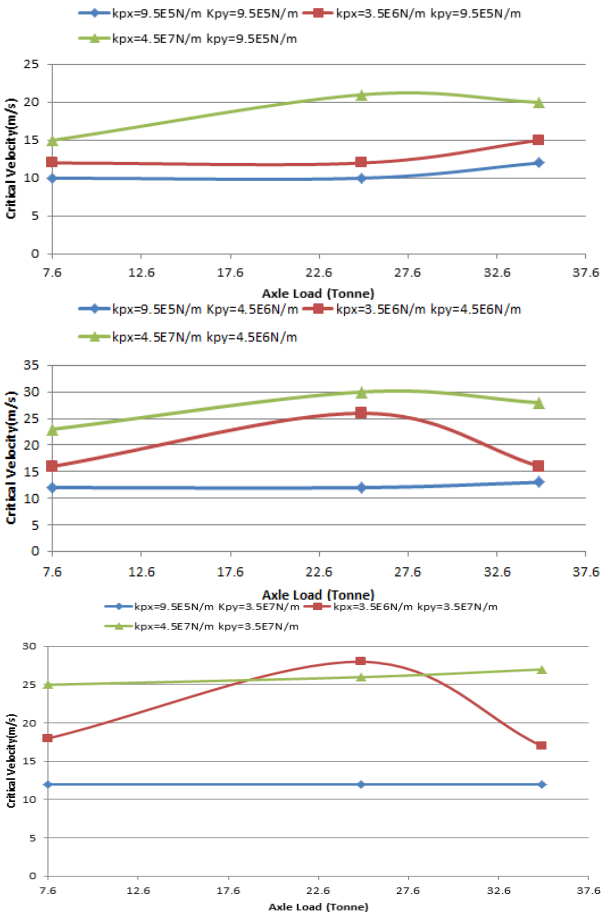

Fig. 6: Critical velocity vs. Axle load for range of Kpx and Kpy

7. Conclusion

In this paper whole numerical model for Railway wagon is used to find the behavior of the dynamics of the empty wagon. The numerical model used having heuristic nonlinear creep model. The vehicle is run at different constant speed on straight Tangent track by varying the primary and secondary spring stiffness for both lateral and longitudinal degrees of freedom. The analysis is run to analyze the hunting stability of the whole vehicle.

REFERENCES:

[1] A.D. De Pater. 1960. The approximate determination of the hunting movement of a railway vehicle by aid of the method of Krylov and Bogoljubow, *Proc. 10th Int. Cong. of Applied Mechanics, Stresa., Appl. Sci. Res. A.*, 10.

[2] N.K. Cooperrider. 1972. The hunting behavior of conventional railway trucks, *ASME J. Engg. Industry*, 94, 752-762. https://doi.org/10.1115/1.3428240.

[3] C. Knudsen, R. Feldberg and A. Jaschinski. 1991. Nonlinear dynamic phenomena in the behavior of a railway wheelset model, *Nonlinear dynamics*, 2, 389-404. https://doi.org/10.1007/BF00045671.

[4] C. Knudsen, E. Slivsgaard, M. Rose, H. True and R. Feldberg. 1994. Dynamics of a model of a railway

wheelset, *Nonlinear Dynamics*, 6, 215-236. https://doi.org/10.1007/BF00044986.

[5] Ch. Kaas-Petersen. 1986. Chaos in a railway bogie, *Acta Mech.*, 61, 89-107. https://doi.org/10.1007/BF01176365.

[6] H. True. 1992. Railway vehicle chaos and asymmetric hunting, *Veh. Syst. Dyn.*, 20, 625-637. https://doi.org/10.1080/00423119208969427.

[7] H. True and C.K. Peterson. 1984. A bifurcation analysis of nonlinear oscillations in railway vehicles, *Proc. 8th IAVSD Dyn. of Vehicles on Roads and Tracks*, 655-665.

[8] H. True. 1989. Chaotic Motion of Railway Vehicles, *Proc. 11th IAVSD Vehicles on Roads and Tracks*, Amsterdam/Lisse, 578-587.

[9] M. Ahmadian and S. Yang. 1998. Effect of system nonlinearities on locomotive bogie hunting stability, *Vehicle System Dynamics: Int. J. Vehicle Mechanics and Mobility*, 29(6), 365-384.

[10] M. Ahmadian and S.P. Yang. 1998. Hopf bifurcation and hunting behavior in a rail wheelset with flange contact, *Nonlinear Dyn.*, 15(1), 15-30. https://doi.org/10.1023/A:1008278713331.

[11] P. Isaksen and H. True. 1997. On the ultimate transition to chaos in the dynamics of Cooperrider's bogie chaos, *Solutions & Fractals*, 8(4), 559-581. https://doi.org/10.1016/S0960-0779(96)00109-9.

[12] C.N. Jensen, M. Golubitsky and H. True. 1999. Symmetry, generic bifurcations, and mode interaction in nonlinear railway dynamics, *Int. J. Bifurcation and Chaos*, 9(7), 1321-1331. https://doi.org/10.1142/S0218127499000924.

[13] A.H. Wicken. 1965. The dynamic stability of railway vehicle wheelsets and bogies having profiled wheels, Int. *J. Solids Structures*, 1, 319-341.

[14] J.J. Kalker. 1980. Review of wheel-rail rolling contact theories, the general problem rolling contact, *Trans. ASME, J Appl. Mech.*, 40, 77-92.

[15] S.M.R. Pena, N. Wilson and D. Di-Brito. 1996. Effects of wheel-rail contact geometry on wheel set steering forces, *Wear*, 191, 204-209. https://doi.org/10.1016/0043-1648(95)06688-8.

[16] R. Kovalev, V.N. Yazykov, G.S. Mikhalchenko and D.Y. Pogorelov. 2003. Railway vehicle dynamics: some aspects of wheel-rail contact modeling and optimization of running gears, *Mech. Based Des. Struct. Mach.*, 31(3), 315-334. https://doi.org/10.1081/SME-120022853.

[17] M. Rajasekaran, V. Hariram and M. Subramanian. 2016. New mass optimization technique to achieve low mass BIW designs using optimal material layout methodology on frontal vehicle crash, *J. Mech. Science and Technology*, 30(12), 3533-3537. https://doi.org/10.1007/s12206-016-1130-5

[18] O. Polach. 2005. Creep forces in simulations of traction vehicles running on adhesion limit, *Wear*, 258, 992-1000. https://doi.org/10.1016/j.wear.2004.03.046.

[19] J. Pombo, J. Ambro´ sio and M. Silva. 2007. A new wheel-rail contact model for railway dynamics, *Veh. Syst. Dyn.*, 45(2), 165-189. https://doi.org/10.1080/00423110600996017.

[20] O. Polach. 1999. A fast wheel-rail forces calculation computer code, *Veh. Syst. Dyn.*, 33, 728-739.

[21] R.F. Harder. 2000. Dynamic modeling and simulation of three-piece freight vehicle suspensions with non-linear frictional behaviour using Adams Rail, *Proc. 5th ADAMS/RAIL User's Conf.*, Haarlem, The Netherlands.

[22] N. Bosso, A. Gugliotta and A. Somà. 2000. Simulation of a freight bogie with friction dampers, *Proc. 5th ADAMS/Rail Users' Conf.*, Haarlem, The Netherlands.

[23] A. Chudzikiewicz. 2000. Simulation of rail vehicle dynamics in Matlab environment, *Veh. Syst. Dyn.*, 33, 107-119. https://doi.org/10.1076/0042-3114(200002)33:2;1-1;FT107.

[24] A. Mohan. 2004. Nonlinear investigation of the effect of primary suspension on the hunting stability of a rail wheelset, *Proc. ASME/IEEE Joint Rail Conf.*, Baltimore, USA. https://doi.org/10.1115/RTD2004-66004.

[25] A. Mohan. 2003. *Nonlinear Investigation of the Use of Controllable Primary Suspensions to Improve Hunting in Railway Vehicles*, MSc Thesis, Virginia Polytechnic Institute and State University, Blacksburg, Virginia.

[26] S. Shukla, R. Gupta and N.S. Vyas. 2009. Parametric study of suspension elements for ride index analysis of an Indian railway freight vehicle, *Int. J. Vehicle Struct. & Sys.*, 1(4), 70-77. http://dx.doi.org/10.4273/ijvss.1.4.03.

[27] J.J. Kalker. Wheel-rail rolling contact theory, *Institute of Railway & Urban Mass Transit Research*, Tongji University, Shanghai, China.

[28] J.J. Kalker. 1973. Simplified theory of rolling contact, *Delft Progr. Rep., Series C: Mechanical and Aeronautical Engineering and Shipbuilding.*

[29] V.K. Garg and R.V. Dukkipati. 1984. *Dynamics of Railway Vehicle Systems*, Academic Press, Toronto.

[30] A.H. Wickens. 2003. *Fundamental of Rail Vehicle Dynamics, Guidance and Stability*, ISBN 90-265-1946-X, Swets & Zeitlinger B.V. Lisse Publishers, The Netherlands.

[31] 1st Course on Advanced vehicle system dynamics, *Int. Centre for Transport Studies, ICTS-PFT Proc. Series*, 4, Edited by: A.D. de Pater & H.B. Pacejka, 25-30th Oct 1982.

[32] *Handbook* of *Railway Vehicle Dynamics*. Edited by Simon Iwnicki. CRC Press 2006.